Clim. Past Discuss., 9, 4987–5018, 2013
www.clim-past-discuss.net/9/4987/2013/
doi:10.5194/cpd-9-4987-2013


Climate of the Past Discussions
Open Access





# Changing correlation structures of the Northern Hemisphere atmospheric circulation from 1000 to 2100 AD

**C. C. Raible[1,2], F. Lehner[1,2], J. F. Gonzalez Rouco[3], and L. Fernandez Donado[3]**

[1]Climate and Environmental Physics, University of Bern, Bern, Switzerland
[2]Oeschger Centre for Climate Change Research, Bern, Switzerland
[3]Instituto de Geociencias (UCM-CSIC),Facultad de CC. Fisicas, Universidad Complutense de Madrid, Madrid, Spain

Received: 24 July 2013 – Accepted: 1 August 2013 – Published: 28 August 2013

Correspondence to: C. C. Raible (raible@climate.unibe.ch)

Published by Copernicus Publications on behalf of the European Geosciences Union.

## Abstract

Atmospheric circulation modes are important concepts to understand the variability of atmospheric dynamics. Assuming their spatial patterns to be fixed, such modes are often described by simple indices derived from rather short observational data sets. The increasing length of reanalysis products allows scrutinizing these concepts and assumptions. Here we investigate the stability of spatial patterns of Northern Hemisphere teleconnections by using the Twentieth Century Reanalysis as well as several control and transient millennium-scale simulations with coupled models. The observed and simulated centers of action of the two major teleconnection patterns, the North Atlantic Oscillation (NAO) and to some extent the Pacific North American (PNA), are not stable in time. The currently observed dipole pattern of the NAO with its center of action over Iceland and the Azores split into a North-South dipole pattern in the western Atlantic and a wave train pattern in the eastern part connecting the British Isles with West Greenland and the Eastern Mediterranean in the period 1940–1969 AD. The PNA centers of action over Canada are shifted southwards and over Florida into the Gulf of Mexico in the period 1915–1944 AD. The analysis further shows that shifts in the centers of action of either telconnection pattern are not related to changes in the external forcing applied in transient simulations of the last millennium. Such shifts in their centers of action are associated with changes in the relation of local precipitation and temperature to the overlying atmospheric mode. These findings further undermine the assumption of stationarity between local climate/proxy variability and large-scale dynamics inherent in proxy-based reconstructions of atmospheric modes and call for a more robust understanding of atmospheric variability on decadal time scales.


## 1 Introduction

The complexity of the large-scale atmospheric flow (Lorenz, 1967) and the associated long-term climate variability are often simplified by characterizing the atmospheric circulation in so-called modes of variability. These modes refer to physically meaningful teleconnection patterns, that connect distant and coherently varying regions with each other, and are often characterized by a time-varying index and a fixed spatial pattern (Stephenson et al., 2003). Since the late 19th century, indices are used to identify regions of coherent climate variability (mainly temperature, precipitation, and pressure) and correlation analysis is used to explore teleconnections (Hann, 1890; Defant, 1924). Such teleconnections originate from in-phase variability that takes place at different locations due to either waves (e.g. Rossby waves) or advection of physical properties (e.g. temperature, humidity, etc.) by air masses (Wanner et al., 2001; Hurrell et al., 2004; Pinto and Raible, 2012).

For the Northern Hemisphere, different teleconnection patterns are identified. Among others the most important for winter are the North Atlantic Oscillation (NAO) and the Pacific North America (PNA) patterns (Wallace and Gutzler, 1981; Barnston and Livezey, 1987). The NAO is the leading mode of the pressure field in the North Atlantic region with two barotropic and anti-correlated centers of action: one over Iceland and the other over Azores extending to the Iberian Peninsula (e.g. Hurrell, 1995). The PNA is mainly manifested in the mid troposphere and represents a wave train with centers over the tropical Pacific, the Aleutian Islands, Northern Canada and Florida in the 500 hPa geopotential height field (Wallace and Gutzler, 1981; Barnston and Livezey, 1987). These pressure patterns modulate the atmospheric flow (e.g. Woollings et al., 2010b) and control cyclone activity and other climate variables, e.g. temperature and precipitation (e.g. Hurrell, 1995; Hurrell and Deser, 2009).

The inherent simplicity of these atmospheric modes, the societal relevance, and the relationships to variables such as temperature and precipitation have attracted the climate proxy and reconstruction community over the last decades. The aim has been to extend the time series of such modes beyond the instrumental period by using proxy data from archives (e.g. tree rings, stalagmites, ice cores) in order to deepen our understanding in the low-frequency variability of such modes (e.g. Casty et al., 2007). This has led to a reasonable number of reconstructions for the NAO (e.g. Luter-





CPD
9, 4987–5018, 2013

bacher et al., 1999; Cook et al., 2002; Mann, 2002; Trouet et al., 2009) and the PNA indices (Moore et al., 2002; Trouet and Taylor, 2010), however, often with contradicting time evolution prior to the instrumental era (Schmutz et al., 2000; Pinto and Raible, 2012). One source of uncertainty arises from the proxies themselves, as temperature-sensitive proxies seem to be less reliable than precipitation sensitive proxy records for reconstructing atmospheric indices (Zorita and Gonzalez-Rouco, 2002). Additionally, regional biases of proxy records and regional representation of proxy sites is important. For instance, Lehner et al. (2012b) recently showed in climate model simulations and reanalysis products that the constraint by only two precipitation sensitive proxies in two different sites used in one reconstruction (Trouet et al., 2009) is insufficient to reliable reconstruct the simulated past NAO behavior. Moreover, the selection of suitable proxy locations in reconstructing atmospheric modes of variability may have been geographically biased toward those regions affected by the NAO in the 20th century (Cook et al., 2002).

One conceptual shortcoming of teleconnection patterns is that their centers of action are often interpreted to be fixed in space, an inherent characteristic of index definitions. Additionally, stationarity in the relation between the proxy records and the atmospheric circulation is a basic assumption of past climate reconstructions of such indices. However, there is growing evidence that this interpretation and the assumption are not always trustworthy. Ulbrich and Christoph (1999) found a systematic northeastward shift of the northern center of action of the NAO in climate model projections for the 21st century, indicating that at least the simulated position of the pressure centers is not stable in time. Investigating the low-frequency characteristics of Northern Hemispheric teleconnection patterns, a series of studies already found structural changes (in shape and position) of these patterns and that these changes are connected to differences in the atmosphere-ocean coupling (Raible et al., 2001, 2004; Luksch et al., 2005). Focussing on longer time scales, Raible et al. (2006) showed evidence that the southern center of action of the NAO is relocated from its present state around the Azores/Lisbon to Central Mediterranean when analyzing European pressure field reconstructions for





CPD
9, 4987–5018, 2013

the past 500 yr (Luterbacher et al., 2002) as well as control simulations with coupled climate models. Franzke and Feldstein (2005) interpreted the teleconnection patterns as continuum of superposed combinations of different atmospheric circulation modes, e.g. for the North Atlantic a combination of the NAO, the East Atlantic (EA) and the Scandinavian (SCA) pattern (Moore et al., 2013). Such combinations can lead to instability in the centers of action and could influence relationships between the large-scale circulation and proxy records (Raible et al., 2006).

The aim of this study is to investigate the spatio-temporal behavior of teleconnection patterns in the Northern Hemisphere for the last 1000 yr in control and transient simulations with two coupled climate models. Thereby the correlation structures are determined by the measure teleconnectivity, first introduced by Wallace and Gutzler (1981). The results are compared with reanalysis data (Compo et al., 2011). The transient simulations are further used to assess a potential response of the spatio-temporal behavior to the external forcing applied. Additionally, impacts of the spatio-temporal behavior of teleconnection patterns on fields relevant for the proxy reconstruction community are discussed.

Section 2 briefly gives an overview of the data sets, the models, and simulations used in this study. The teleconnection patterns are introduced and their spatial variability is discussed in Sect. 3. Then, the impact of the changing correlation structures on known proxy sites is illustrated, highlighting potential limitations of the ability of current proxies to reconstruct such changes (Sect. 4). Finally, conclusive remarks are presented in Sect. 5.

## 2 Data, models, and experimental design

In this study we use the Twentieth Century Reanalysis (TCR, version 2; Compo et al., 2006, 2011, NOAA/OAR/ESRL PSD, Boulder, Colorado, USA). These data are generated at T63 horizontal resolution (i.e. a triangular spectral truncation at wave number 63) and provided on a regular grid of $2.5^{\circ} \times 2.5^{\circ}$. The data are interpolated to T30/T31





CPD
9, 4987–5018, 2013

(roughly 3.75° × 3.75°) to be comparable with the model data. The TCR reanalysis consists of an ensemble of 56 members and the ensemble mean for the period 1871–2010.

Besides the reanalysis product, the study bases on model results from two different fully coupled climate models. The first model is the Climate Community System Model, Version 3 (CCSM3) developed by the NCAR (Collins et al., 2006), and consists of the four components atmosphere, ocean, land surface, and sea ice, all coupled without flux adjustments. To generate ensemble simulations the lowest resolution setting is selected. The atmospheric component has 26 $\sigma$-pressure levels and a horizontal resolution of T31. The land surface shares the same horizontal resolution as the atmosphere. The ocean component has 25 unevenly spaced depth levels and a nominal horizontal resolution of 3° (refined around Greenland and near the equator to approximately 0.9°). The thermodynamic and dynamic sea ice component has the same horizontal resolution as the ocean component. To assess the role of the resolution T85 in the atmosphere and nominal 1° in the ocean is used for one simulation.

The second model (denoted as ECHO-G in the following) consists of four model components, however coupled with an annual mean flux correction scheme for heat and freshwater that average out globally (Legutke and Voss, 1999). The atmospheric component is the fourth version of the European Centre model of Hamburg (ECHAM4) with a horizontal resolution of T30 and 19 $\sigma$-pressure levels (Roeckner et al., 1996). The ocean component is the Hamburg ocean model in primitive equations (HOPE) with a horizontal resolution of 2.8° × 2.8° and 20 unevenly spaced vertical depth levels (Wolff et al., 1997). Moreover, a land surface and a thermodynamic sea ice component are part of the model system.

Both models are used to perform (i) control simulations (Ctrl) with constant external forcing, and (ii) transient simulations (TR1a–TR4a and TR1b with the CCSM3; Erik I and II with ECHO-G) with time-varying external forcing as boundary condition (Table 1). As control simulations, four simulations with the CCSM3 are available with perpetual 1000, 1500, and 1990 AD forcing. Details of the climatology and biases of the 1990 AD simulation in T31 can be found in Yeager et al. (2006). Additionally, a Ctrl simulation for 1990 AD conditions with T85 provided by the NCAR is used to show the influence of the resolution on the results. The Ctrl1000 and Ctrl1500 simulations are discussed in Yoshimori et al. (2010) and Hofer et al. (2011). For ECHO-G, a Ctrl1900 simulation is used. Its climatology is presented in Legutke and Voss (1999) and the variability of the Northern Hemisphere large-scale atmospheric circulation is investigated by Raible et al. (2001, 2004, 2005), Zorita et al. (2003), and Luksch et al. (2005).

Five transient simulations with CCSM3 are used covering the last five centuries up to the last millennium. An ensemble of four simulations (TRa1 to TRa4) is integrated from 1500 to 2000 AD, where the initial states are obtained from different years of the Ctrl1500 simulation. One simulation (TRb1) spans over the entire millennium, with an initial state from the Ctrl1000 simulation. For all five simulations, the same external forcing is applied, i.e. greenhouse gas (GHG) concentrations, volcanic aerosols (in the stratosphere), and solar irradiance (summarized in Fig. 1, black lines). Further details of the simulations and the forcing functions are presented in Yoshimori et al. (2010), Hofer et al. (2011) and Lehner et al. (2012a,b). All simulations are extended to 2099 AD using the SRES A2 scenario (IPCC, 2001, 2007). Two ECHO-G transient simulations are used, one with rather warm initial conditions (ERIK-I) and one with comparatively colder initial conditions (ERIK II). The external forcing is slightly different from the CCSM3 simulation (Fig. 1). In particular, the volcanic forcing is added to the solar irradiance; thus it only takes the direct shortwave effect of volcanic eruptions into account. As in the case of CCSM3 simulations, one simulation is extended to 2100 AD using the SRES A2 scenario. Details of these simulations are presented by Gonzalez-Rouco et al. (2003, 2006, 2009) and Zorita et al. (2005). The simulations of both model setups are also compared with reconstructions and other simulations of the last millennium by assessing the temperature response to the external forcing in Fernandez-Donado et al. (2013). Note that the variability of the solar forcing used to drive both the CCSM3 and ECHO-G simulations, is rather large, i.e. total solar irradiance changes between the Late Maunder Minimum (1680–1715 AD) and the late 20th century are 0.23 % (CCSM3) and 0.29 % (ECHO-G), as presented in the multi-model comparison by Fernandez-Donado et al. (2013).

## 3 Northern Hemisphere teleconnection patterns

In this section we first compare the long-term mean behavior of the model simulations with observations wherewith the classical teleconnection patterns are introduced and model biases in the correlation patterns are discussed. The teleconnections are analyzed by teleconnectivity maps based on 500 hPa geopotential height (hereafter Z500) for winter months December to February (DJF), as first introduced by Wallace and Gutzler (1981). The teleconnectivity is a field of anti-correlation based on the geopotential height in 500 hPa. Correlating one grid point with all others the strongest negative correlation is searched and denoted at this grid point. Assessing all grid points by this procedure leads to a field of negative correlation where the areas of stronger negative correlation correspond to centers of action of teleconnection patterns. These centers of action are combined by teleconnection axes (Wallace and Gutzler, 1981; Raible et al., 2006). The method is applied to monthly DJF data. Prior to the application of the teleconnectivity method the seasonal cycle is removed. In the second part of this section the time-varying behavior of the correlation patterns is presented.

### 3.1 Long-term mean

Applying the method of Wallace and Gutzler (1981) to the Z500 fields of the TCR data shows the well-known teleconnection patterns for the current observational period from 1971–2000 AD. Teleconnectivity regions corresponding to the North Atlantic Oscillation (NAO) pattern, the West Pacific (WP) pattern, the Pacific North America (PNA) pattern, an area over Siberia and one connecting the eastern Mediterranean with Central Europe are identified. The latter shows weaker anti-correlations than for the aforementioned regions (Fig. 2a). Using the entire period from 1871 to 2008 AD to





CPD
9, 4987–5018, 2013

deduce the teleconnections shows that the anti-correlations for all patterns are slightly reduced (Fig. 2b). In particular over the North Atlantic region this reduction is observed, but more importantly also the teleconnection patterns change in such a way that the more eastern position of the centers of action of the NAO in the period 1971–2000 AD (Fig. 2a) is shifted to the central Atlantic (Fig. 2b).

The simulated NAO-type teleconnection patterns substantially deviate from the observed one. In the CCSM3 Ctrl experiment, the main teleconnection pattern is shifted southwards with centers of action located South of the British Islands and South of the Canary Islands and Northern Africa (Fig. 2c). In the western part of the North Atlantic, CCSM3 displays a weaker NAO-type pattern. The ECHO-G Ctrl experiment shows a similar southward displacement as CCSM3, however omitting a center over Northern Africa. A pattern in the western part of the North Atlantic is not identified, but the Ctrl simulation shows the pattern connecting Central Europe with the Eastern Mediterranean region as in the observations. The simulated teleconnectivity maps of the control experiments exhibit agreement over the Pacific and Siberia (Fig. 2c, d). The WP and the PNA patterns are nicely represented in all Ctrl experiments with some minor deviations in CCSM3, which simulates a North-South dipole structure in the eastern part of the Pacific and a slight westward shift of the Florida center of the PNA pattern. The ECHO-G Ctrl experiment slightly underestimates the anti-correlation of the WP pattern.

The transient experiments of each model configuration resemble the biases of the Ctrl experiments. Thus, the model simulations exhibit in some areas substantial biases in the correlation patterns and may only be partly able to correctly simulate teleconnection patterns.

### 3.2 Time behavior of teleconnection patterns

Differences in teleconnectivity between the entire TCR and the period from 1971–2000 AD already hints at a potential change of correlation structures over time. To investigate the time dependence of the teleconnection patterns, the teleconnectivity based on Z500 is deduced in a 30 yr running window. The agreement or disagreement with the current observed patterns is measured by pattern correlation between these patterns (reference period: 1971–2000 AD) and patterns based on the running 30 yr periods. The pattern correlation index is derived for two areas: the North Atlantic European region (100° W–50° E, 0°–90° N) and the North Pacific America region (230° W–70° W, 0°–90° N). A pattern correlation index of $r = 1$ means that the teleconnection map of, e.g. a past 30 yr period, perfectly matches with the current reference teleconnection map. The pattern correlation is a very demanding measure, as tests in the model world and the reanalysis shows. Shifting a teleconnection pattern by, e.g. 2 grid points will deteriorate the pattern correlation from $r = 1$ to roughly $r = 0.85$. Thus, we consider the resulting time series of pattern correlation to give evidence of periods of agreement with the current state for high positive pattern correlation or disagreement for low or even negative pattern correlation, but we do not expect to reach $r = 1$.

The pattern correlation index time series of TCR shows disagreement with the reference teleconnection patterns already in the 20th century for the North Atlantic region (Fig 3a). In the period from 1940–1969 AD the pattern correlation $r$ is below 0.5 hinting at the correlation structure experiencing a substantial change during this time. Going further back in time, the agreement of the teleconnection patterns with the reference pattern increases to levels of 0.6 to 0.7 in TCR. The data quality and amount is reduced in the early part of this reanalysis product, possibly affecting the ensemble mean. Therefore, each ensemble member of the reanalysis is investigated separately. The results of each ensemble member confirm the aforementioned finding of a better agreement and highlight the robustness of a disagreeing period from 1940–1969 AD. The climate model simulations show a different picture (Fig 3b–e). Overall the pattern correlation is reduced, which indicates that the climate model simulations may have problems to correctly simulate the teleconnection patterns as mentioned previously. Still, there are also differences between the models. CCSM3 shows a pattern correlation range of approximately −0.2 to 0.7 (with a mean of 0.2) whereas ECHO-G has a range of roughly 0 to 0.8 (mean of 0.4). This means that the model biases





CPD
9, 4987–5018, 2013

in CCSM3 are stronger than in ECHO-G. Moreover, increasing the resolution to T85 shows no substantial difference for the CCSM3 model family. Despite these biases all simulations show decadal-scale variability of periods with agreement ($r > 0.6$) and disagreement (low or negative $r$). Comparing the Ctrl simulations with the corresponding transient simulations we find no difference in the range of pattern correlation, nor a difference in the variability of the time series. Moreover, the variability of the pattern correlation indices of the transient simulations shows no coherency among each other and is unrelated to changes in the external forcing for both models (Fig. 1). This holds true for the future as well when no systematic response to the increased forcing from greenhouse gases is detectable. Also the mean climate state seems to be irrelevant for the variability of agreement as illustrated for the CCSM3 model by the different Ctrl simulations. None of these simulations show a substantial difference with respect to the behavior of periods of agreement and disagreement.

For the Pacific region the TCR teleconnection patterns show a decrease in agreement with the reference pattern when going back in time (Fig. 4a). The lowest values of the pattern correlation index are identified at the beginning in the period 1871 to 1900 AD. However, when analyzing the ensemble members separately we find that the time series based on the ensemble mean exceeds the range given by the ensemble members. This is a hint that this reanalysis product is not well constrained by observations in the Pacific in the early period and thus the results for this period are not trustworthy and could overemphasize the disagreement. Focusing on the period 1915–2010 AD, where the reanalysis is better constrained by observations, the pattern correlations show some change from 1 to roughly 0.7. This range is smaller than in the the North Atlantic, giving a first hint that more stable and time-independent teleconnection patterns are active in the Pacific than in the Atlantic. The model simulations confirm this result, showing a reduced range of the corresponding pattern correlation indices for the Pacific (Fig. 4b–e). As for the Atlantic, the simulations show biases for the Pacific. The mean pattern correlation is $\sim 0.4$ for the CCSM3 and $\sim 0.6$ for ECHO-G. Again, using a higher resolution in CCSM3 shows no substantial improvement in





CPD
9, 4987–5018, 2013

simulating the teleconnections compared with the T31 control simulations. Further, the time series of the Pacific show similar behavior in the Ctrl and transient simulations and no external forcing imprint (also under future GHG forcing), similar to findings in the Atlantic.

Thus, we conclude that the temporal variability of simulated teleconnections of the Northern Hemisphere North of 20° N is not different from internal climate variability for the last 1000 yr. Moreover, using a different window size (e.g. 40 yr) exhibits that the results are not affected (not shown).

Further insights in the differences of the correlation patterns are gained by a composite analysis of the 30 yr running window teleconnectivity patterns. Therefore, the time series of pattern correlation are used as index. The average over all teleconnectivity maps is taken, that exceed two standard deviations of the index (denotes as high pattern correlation or agreement with the reference teleconnectivity pattern) or fall below two standard deviations of the index (denotes as low pattern correlation or disagreement with the reference teleconnectivity pattern). These composites illustrate the characteristic teleconnection patterns of agreement and disagreement with the reference pattern. However, it shall be mentioned that the mean of different teleconnectivity patterns is not necessarily meaningful. Only if the absolute range of teleconnectivity is not strongly affected (i.e. the mean teleconnectivity pattern has a similar range as a single pattern of a 30 yr period) the application of a composite analysis is trustworthy. As increasing the resolution of CCSM3 shows no difference the T85 simulation is excluded from this analysis.

The composite of the high pattern correlation index in the North Atlantic resembles the observed reference pattern as expected in reanalysis and models (Fig. 5, left column). Moreover, the range of the teleconnectivity of the composites is similar to the observed reference period and indicates that the variability between the composite members is low and the identified patterns are therefore a robust description of the correlation pattern for high index conditions. All model simulations show the well-known dipole pattern of the NAO. Again, CCSM3 shows some stronger deviations when com-





CPD
9, 4987–5018, 2013

paring Fig. 5c, g with observations (Fig. 5a) where a pattern connecting North Africa with a center located North of Spain is identified in the simulations. This explains the lower maximum pattern correlation found for CCSM3. The ECHO-G simulations agree better than CCSM3, but still overemphasize the teleconnectivity in Central Europe, which is connected with the Eastern Mediterranean (Fig. 5e, i). Concerning situations of disagreement in the TCR (the period 1940–1969 AD) the NAO-type teleconnection is shifted to the West and a new wave train-like teleconnection pattern connecting the British Islands with West Greenland and the Eastern Mediterranean is detected (Fig. 5b). The simulated composites of the low pattern correlation index in North Atlantic partly resembles the observed patterns (Fig. 5d, f, h, j). CCSM3 simulates the western shift of the NAO-type pattern, but does not show the pattern over Europe. Instead the model shows the tripole pattern with centers of action located South of the British Islands and South of the Canary Islands and Northern Africa already discussed in Sect. 3.1 as model bias. In contrast, The ECHO-G simulations identifies the European-Eastern Mediterranean pattern, however fails to generate the western shift of the NAO-type pattern. Instead the NAO-type pattern is shifted southwards by roughly 10° reflecting the biases of ECHO-G (Sect. 3.1).

The North Pacific composite of the high pattern correlation index resembles the observed reference pattern from 1971–2000 AD (Fig. 6, left column). The WP and the PNA pattern are found in all simulations with only minor deviations of the locations of the centers of action (i.e. the CCSM3 composite shows a tendency to split the tropical center of the PNA pattern into two; Fig. 6c). Again this is expected as the pattern correlation indices are on average higher than for the Atlantic (Figs. 3 and 4). The observed disagreeing period (1915–1944 AD, Fig. 6b) exhibits a change in the PNA pattern shifting its centers of action over Canada southwest and over Florida to the Gulf of Mexico. Moreover, the WP pattern is shifted to the north west. Concerning the model simulations for the disagreeing patterns we find that the PNA pattern is only weakly affected with a slight shift of the Florida center of action. The main difference is found in the western part of the Pacific where the model simulations lose the WP pattern. Additionally, CCSM3 simulates a split of the tropical center of the PNA, which is potentially a model bias (Sect. 3.1). As for the Atlantic, the Pacific composites of the model simulations show a similar range of teleconnectivity as the observations, therefore giving evidence of the robustness of these patterns. Overall the changes in the North Pacific are less pronounced than in the Atlantic favoring that teleconnections in the Pacific appear to be more stable than in the Atlantic.

## 4 Implications for proxy reconstructions

Proxy-based reconstructions of past atmospheric circulation patterns rely, as mentioned before, on the assumption of stationarity in the relationship between a proxy signal and the corresponding atmospheric circulation. It has been illustrated in a number of studies that this assumption, primarily derived from late twentieth century data, might not hold if one considers longer time scales (e.g. Lehner et al., 2012b). Moreover, within the observational period as well as in model simulations, the teleconnectivity patterns in both Atlantic and Pacific change over time (as demonstrated in Sect. 3). This means that what are currently (1971–2000 AD) considered the dominant patterns of teleconnectivity (e.g. NAO and PNA) do not necessarily look the same in other time periods of equal length. Therefore one can expect that, along with changes in the teleconnectivity patterns, changes in the correlation strength of a fixed proxy site with the overlying atmospheric circulation occur.

The period of maximum disagreement with the reference teleconnectivity pattern in the Atlantic in TCR (1940–1969 AD) features the NAO-like dipole, but substantially shifted to the West (Fig. 5b). We consider this our hypothetical reference teleconnectivity pattern and derive an index, the West Atlantic Dipole (WADP), based on the normalized Z500 time series from the two new centers of action at 39° N/19° W and 68° N/19° W. Similarly, an index is defined for the wave train that emerges in the Eastern Atlantic region during the disagreement period of 1940–1969 AD: $0.5 \cdot$ Z500 (50° N/ 7° E) $-0.25 \cdot$ Z500 (32° N/ 37° E) $-0.25 \cdot$ Z500 (80° N/ 29° W), hereafter AWAVE. These

WADP and AWAVE indices can, just as the classical NAO index, be correlated with fields of precipitation, temperature, or sea level pressure to determine regions of high or low correlation with this index (e.g. Hurrell and Loon, 1997). These correlation maps are then subtracted from the correlation maps derived from the original reference period 1971–2000 AD when the classical NAO (Z500 Azores−Iceland) is present (Fig. 5a). In this way, regions are identified where the relationship of a proxy site with the dominant teleconnectivity pattern changes with the chosen reference period.

Figure 7 displays regions where a sign change in correlation occurs when the correlation map of WADP and AWAVE are subtracted from the one of NAO. It is revealed that existing precipitation proxy sites on the North American East coast and in middle- to northern Europe have differing relationships to the overlying dominant atmospheric circulation depending on the time period in question. Similarly, existing temperature proxy sites in North America or in Greenland as well as sea level pressure proxy sites in middle- to northern Europe are affected by such sign changes in correlation. The proxies used to illustrate potentially affected sites are from or compiled in Mann et al. (2008), Küttel et al. (2010), Trouet et al. (2009), Trouet and Taylor (2010), Cook et al. (1998), and Glueck and Stockton (2001) and are obtained from NOAA's Paleoclimatology database (www.ncdc.noaa.gov/paleo/data.html). Note that the proxy list is not exhaustive but serves as illustrative example.

The same analysis is conducted in the Pacific defining an index for the shifted PNA pattern: $0.25 \cdot (\mathrm{Z500}\,(19^\circ\,\mathrm{N};\ 173^\circ\,\mathrm{W}) - \mathrm{Z500}\,(53^\circ\,\mathrm{N};\ 169^\circ\,\mathrm{W}) + \mathrm{Z500}\,(45^\circ\,\mathrm{N};\ 113^\circ\,\mathrm{W}) - \mathrm{Z500}\,(30^\circ\,\mathrm{N};\ 98^\circ\,\mathrm{W}))$. Then again, correlation maps of this shifted PNA index during the time period of maximum disagreement, 1915–1944 AD, are subtracted from the ones of the classical PNA, which is defined as $0.25 \cdot (\mathrm{Z500}\,(17^\circ\,\mathrm{N};\ 173^\circ\,\mathrm{W}) - \mathrm{Z500}\,(46^\circ\,\mathrm{N};\ 165^\circ\,\mathrm{W}) + \mathrm{Z500}\,(58^\circ\,\mathrm{N};\ 105^\circ\,\mathrm{W}) - \mathrm{Z500}\,(28^\circ\,\mathrm{N};\ 83^\circ\,\mathrm{W}))$ during the reference time period 1971–2000 AD (Fig. 8). While sign changes in the relationship between proxy and teleconnectivity index occur here as well, none relate to regions where a significant correlation exists or emerges. This confirms the conclusions in Sect. 3 as to the more stable nature of teleconnectivity patterns in the Pacific (e.g. PNA) as compared to the Atlantic (e.g. NAO).

## 5 Conclusions

Changing correlation structures of the Northern Hemisphere atmospheric circulation are investigated for the period 1000–2100 AD using reanalysis data and different sets of millennium-long control and externally forced simulations with two coupled climate models. The observed and simulated centers of action of the major teleconnection patterns NAO and PNA are not stable in time. In particular, the observed patterns in the North Atlantic sector vary strongly showing a splitting in a North-South dipole in the western part of the North Atlantic and a wave train pattern in the Eastern part and over Europe during some periods. The observed, structural changes in the North Pacific and over North America are smaller compared to the North Atlantic. The findings of the North Atlantic are in line with earlier studies assuming a non-stationarity of the centers of action of the NAO (Raible et al., 2001, 2006), a continuum of teleconnection patterns (Franzke and Feldstein, 2005) and recently a postulated changing linear combination of the leading modes of variability in the North Atlantic (Moore et al., 2013).

Expanding the analysis further back in time and into the future with model simulations complements the picture, although model biases are evident in simulating the teleconnection patterns and the locations of their centers of action. These biases remain even when the resolution is increased, as illustrated by one model set up. This is a hint that climate models still suffer of under-representing important atmospheric processes such as blocking action (Woollings et al., 2010a; Buehler et al., 2011) or stratosphere-troposphere interaction (e.g. Kodera et al., 1996) and resembles our incomplete understanding of atmosphere dynamics. Despite these biases, the model simulations show strong variability of the teleconnection patterns over time and to some extent similar deviations are found in the reanalysis data for the past 130 yr. Comparing the transient simulations with external forcing and with the behavior of the corresponding control simulations shows that the variability of teleconnections of the Northern Hemisphere North of 20° N over time is not different from internal climate variability for the last 1000 yr. Even for the rather high external forcing of the A2 scenario for the future, a systematic change is not found. This contradicts earlier findings by Ulbrich and Christoph (1999) who suggested a north-eastwards shift of the NAO centers of action under greenhouse gas induced warming. Whether this is a robust finding is questionable as our ensemble of opportunity encompasses only three simulations and should be assessed in a wider pool of simulations such as CMIP5 (Taylor et al., 2012).

The reasons for changing teleconnection structures are less understood. The periods in the reanalysis where teleconnection patterns disagree with the current locations resemble to some extent periods with different atmosphere-ocean coupling. Raible et al. (2001) identified periods during which decadal-scale variability of the NAO coincides with strong coupling of the atmosphere to the ocean underneath, whereas periods dominated by interannual variability seem to be related to tropical SST changes in the Pacific. In line with these changes the coupling between Atlantic and Pacific is found to be variable over time (Raible et al., 2004; Luksch et al., 2005; Pinto et al., 2011). Other reasons like stratosphere-troposphere interaction (Kodera et al., 1996; Woollings et al., 2010a) or sea-ice interaction with the atmosphere (e.g. Lehner et al., 2013) are also potential drivers of such changes, but clearly this needs future research foci.

Another important conclusion concerns the implication for reconstructions of modes of variability back in time. Such reconstructions rely on a stationary relationship between the proxy site and the overlying atmospheric mode, thereby also implying that the dominant atmospheric mode does not change over time. We show that changes in the correlation between proxy sites and teleconnectivity indices occur already in the twentieth century. This indicates that some proxy sites may be used to reconstruct a known atmospheric mode (e.g. the NAO as we know it from 1971–2000), yet they do not necessarily allow to determine whether this was actually the dominant mode and how the atmospheric teleconnections looked like during a specific time period.





CPD
9, 4987–5018, 2013

The Atlantic appears to be more delicate with a number of proxy sites affected by a sign change of correlation between proxy and atmospheric mode. Together with other studies (e.g. Lehner et al., 2012b) these results advise future reconstructions of atmospheric modes to thoroughly test and carefully select the proxies to be used and most importantly to cautiously interpret their results with respect to what part of past climate variability can be explained by a specific reconstruction.

*Acknowledgements.* This work is supported by the Sinergia project FUPSOL funded by the Swiss National Science Foundation. 20th Century Reanalysis data is provided by the NOAA/OAR/ESRL PSD, Boulder, Colorado, USA (from their Web site at http://www.esrl.noaa.gov/psd/). The CCSM3 simulations are performed on the super computing architecture of the Swiss National Supercomputing Centre (CSCS). LFD and JFGR were supported by CGL 2011-29677-602-02, CGL 2011-29672-602-01, and the FPU grant AP2009-4061.

## References

Barnston, A. G. and Livezey, R. E.: Classification, seasonality and persistence of low-frequency atmospheric circulation patterns, Mon. Weather Rev., 115, 1825–1850, 1987. 4989

Buehler, T., Raible, C. C., and Stocker, T. F.: On the relation of extreme North Atlantic blocking frequencies, cold spells, and droughts in ERA-40 in winter, Tellus, 63, 212–222, 2011. 5002

Casty, C., Raible, C. C., Stocker, T. F., Wanner, H., and Luterbacher, J.: European climate pattern variability since 1766, Clim. Dynam., 29, 791–805, 2007. 4989

Collins, W. D., Bitz, C. M., Blackmon, M. L., Bonan, G. B., Bretherton, C. S., Carton, J. A., Chang, P., Doney, S. C., Hack, J. J., Henderson, T. B., Kiehl, J. T., Large, W. G., McKenna, D. S., Santer, B. D., and Smith, R. D.: The Community Climate System Model version 3 (CCSM3), J. Climate, 19, 2122–2143, 2006. 4992

Compo, G., Whitaker, J., and Sardeshmukh, P.: Feasibility of a 100-year reanalysis using only surface pressure data, B. Am. Meteorol. Soc., 87, 175–190, 2006. 4991

Compo, G. P., Whitaker, J. S., Sardeshmukh, P. D., Matsui, N., Allan, R. J., Yin, X., Gleason Jr., B. E., Vose, R. S., Rutledge, G., Bessemoulin, P., Broennimann, S., Brunet, M., Crouthamel, R. I., Grant, A. N., Groisman, P. Y., Jones, P. D., Kruk, M. C., Kruger, A. C., Marshall, G. J., Maugeri, M., Mok, H. Y., Nordli, O., Ross, T. F., Trigo, R. M., Wang, X. L., Woodruff, S. D., and Worley, S. J.: The Twentieth Century Reanalysis Project, Q. J. Roy. Meteorol. Soc., 137, 1–28, 2011. 4991

Cook, E. R., D'Arrigo, R. D., and Briffa, K. R.: A reconstruction of the North Atlantic oscillation using tree-ring chronologies from North America and Europe, Holocene, 21, 1453–1465, 1998. 5001

Cook, E. R., D'Arrigo, R. D., and Mann, M. E.: A well-verified, multiproxy reconstruction of the winter North Atlantic Oscillation index since AD 1400, J. Climate, 15, 1754–1764, 2002. 4990

Defant, A.: Die Schwankungen der atmosphärischen Zirkulation über dem nordatlantischen Ozean im 25-jährigen Zeitraum 1881–1905, Geogr. Ann., 6, 13–41, 1924. 4989

Fernández-Donado, L., González-Rouco, J. F., Raible, C. C., Ammann, C. M., Barriopedro, D., García-Bustamante, E., Jungclaus, J. H., Lorenz, S. J., Luterbacher, J., Phipps, S. J., Servonnat, J., Swingedouw, D., Tett, S. F. B., Wagner, S., Yiou, P., and Zorita, E.: Large-scale temperature response to external forcing in simulations and reconstructions of the last millennium, Clim. Past, 9, 393–421, doi:10.5194/cp-9-393-2013, 2013. 4993, 4994

Franzke, C. and Feldstein, S. B.: The continuum and dynamics of Northern Hemisphere teleconnection patterns, J. Atmos. Sci., 62, 3250–3267, 2005. 4991, 5002

Glueck, M. F. and Stockton, C. W.: Reconstruction of the North Atlantic Oscillation, 1429–1983, Int. J. Climatol., 21, 1453–1465, 2001. 5001

Gonzalez-Rouco, F., von Storch, H., and Zorita, E.: Deep soil temperature as proxy for surface air-temperature in a coupled model simulation of the last thousand years, Geophys. Res. Lett., 30, 2116, doi:10.1029/2003GL018264, 2003. 4993

Gonzalez-Rouco, J. F., Beltrami, H., Zorita, E., and von Storch, H.: Simulation and inversion of borehole temperature profiles in surrogate climates: Spatial distribution and surface coupling, Geophys. Res. Lett., 33, L01703, doi:10.1029/2005GL024693, 2006. 4993

González-Rouco, J. F., Beltrami, H., Zorita, E., and Stevens, M. B.: Borehole climatology: a discussion based on contributions from climate modeling, Clim. Past, 5, 97–127, doi:10.5194/cp-5-97-2009, 2009. 4993

Hann, J.: Zur Witterungsgeschichte von Nord-Grönland, Westküste, Meteorl. Z., 15, 787–799, 1890. 4989

Hofer, D., Raible, C. C., and Stocker, T. F.: Variations of the Atlantic meridional overturning circulation in control and transient simulations of the last millennium, Clim. Past, 7, 133–150, doi:10.5194/cp-7-133-2011, 2011. 4993

Hurrell, J. W.: Decadal trends in the North Atlantic Oscillation: Regional temperatures and precipitation, Science, 269, 676–679, 1995. 4989

Hurrell, J. W. and Deser, C.: North Atlantic climate variability: The role of the North Atlantic Oscillation, J. Mar. Syst., 78, 28–41, 2009. 4989

Hurrell, J. W. and Loon, H. V.: Decadal variations in climate associated with the North Atlantic Oscillation, Clim. Change, 36, 301–326, 1997. 5001

Hurrell, J. W., Hoerling, M. P., Phillips, A., and Xu, T.: Twentieth century North Atlantic climate change. Part I: Assessing determinism, Clim. Dynam., 23, 371–389, 2004. 4989

IPCC: Climate Change 2001: The Scientific Basis. Contribution of Working Group I to the Third Assessment Report of the Intergovernmental Panel on Climate Change, Cambridge University Press, Cambridge, UK and New York, NY, USA, 2001. 4993

IPCC: Climate Change 2007: The Physical Science Basis. Contribution of Working Group I to the Forth Assessment Report of the Intergovernmental Panel on Climate Change, Cambridge University Press, Cambridge, UK and New York, NY, USA, 2007. 4993

Kodera, K., Chiba, M., Koide, H., Kitoh, A., and Nikaidou, Y.: Interannual variability of the winter stratosphere and troposphere in the Northern Hemisphere, J. Meteorol. Soc. Jpn, 1996. 5002, 5003

Küttel, M., Xoplaki, E., Gallego, D., Luterbacher, J., Garcia-Herrera, R., Allan, R., Barriendos, M., Jones, P. D., Wheeler, D., and Wanner, H.: The importance of ship log data: Reconstructing North Atlantic, European and Mediterranean sea level pressure fields back to 1750, Clim. Dynam., 34, 1115–1128, 2010. 5001

Legutke, S. and Voss, R.: The Hamburg Atmosphere-Ocean Coupled circulation model ECHO-G, Tech. Rep. 18, Deutsches Klimarechenzentrum, Hamburg, Germany, 62 pp., 1999. 4992, 4993

Lehner, F., Raible, C. C., Hofer, D., and Stocker, T. F.: The freshwater balance of polar regions in transient simulations from 1500 to 2100 AD using a comprehensive coupled climate model, Clim. Dynam., 39, 347–363, 2012a. 4993

Lehner, F., Raible, C. C., and Stocker, T. F.: Testing the robustness of a precipitation proxy-based North Atlantic Oscillation reconstruction, Quaternary Sci. Rev., 45, 85–94, 2012b. 4990, 4993, 5000, 5004

Lehner, F., Born, A., Raible, C. C., and F, S. T.: Amplified inception of European Little Ice Age by sea ice-ocean-atmosphere feedbacks, J. Climate, doi:10.1175/JCLI-D-12-00690.1, in press, 2013. 5003

Lorenz, E. N.: The nature and theory of the general circulation of the atmosphere, Tech. rep., WMO-No. 218, TP 115, 161 pp., 1967. 4988

Luksch, U., Raible, C. C., Blender, R., and Fraedrich, K.: Cyclone track and decadal Northern Hemispheric regimes, Meteorol. Z., 14, 747–753, 2005. 4990, 4993, 5003

Luterbacher, J., Schmutz, C., Gyalistras, D., Xoplaki, E., and Wanner, H.: Reconstruction of monthly NAO and EU indices back to AD 1675, Geophys. Res. Lett., 26, 2745–2748, 1999. 4989

Luterbacher, J., Xoplaki, E., Dietrich, D., Jones, P. D., Davies, T. D., Portis, D., Gonzalez-Rouco, J. F., von Storch, H., Gyalistras, D., Casty, C., and Wanner, H.: Extending North Atlantic Oscillation reconstructions back to 1500, Atmos. Sci. Lett., 2, 114–124, 2002. 4991

Mann, M. E.: Large-scale climate variability and connections with the Middle East in past centuries, Clim. Change, 55, 287–314, 2002. 4990

Mann, M. E., Zhang, Z. H., Hughes, M. K., Bradley, R. S., Miller, S. K., Rutherford, S., and Ni, F. B.: Proxy-based reconstructions of hemispheric and global surface temperature variations over the past two millennia, Proc. Natl. Acad. Sci. USA, 105, 13252–13257, 2008. 5001

Moore, G., Holdsworth, G., and Alverson, K.: Climate change in the North Pacific region over the past three centuries, Nature, 420, 401–403, 2002. 4990

Moore, G. W. K., Renfrew, I. A., and Pickart, R. S.: Multidecadal mobility of the North Atlantic Oscillation, J. Climate, 26, 2453–2466, 2013. 4991, 5002

Pinto, J. and Raible, C. C.: Past and recent changes in the NAO, Interdisciplinary Reviews Climate Change, 3, 79–90, 2012. 4989, 4990

Pinto, J. G., Reyers, M., and Ulbrich, U.: The variable link between PNA and NAO in observations and in multi-century CGCM simulations, Clim. Dynam., 36, 337–354, 2011. 5003

Raible, C. C., Luksch, U., Fraedrich, K., and Voss, R.: North Atlantic decadal regimes in a coupled GCM simulation, Clim. Dynam., 18, 321–330, 2001. 4990, 4993, 5002, 5003

Raible, C. C., Luksch, U., and Fraedrich, K.: Precipitation and Northern Hemisphere regimes, Atmos. Sci. Lett., 5, 43–55, 2004. 4990, 4993, 5003

Raible, C. C., Stocker, T. F., Yoshimori, M., Renold, M., Beyerle, U., Casty, C., and Luterbacher, J.: Northern Hemispheric trends of pressure indices and atmospheric circulation patterns in observations, reconstructions, and coupled GCM simulations, J. Climate, 18, 3968–3982, 2005. 4993

Raible, C. C., Casty, C., Luterbacher, J., Pauling, A., Esper, J., Frank, D. C., Büntgens, U., Roesch, A. C., Wild, M., Tschuck, P., Vidale, P.-L., Schär, C., and Wanner, H.: Climate variability – observations, reconstructions and model simulations, Clim. Change, 79, 9–29, 2006. 4990, 4991, 4994, 5002, 5012

Roeckner, E., Arpe, K., and Bengtsson, L.: The atmospheric General Circulation Model ECHAM-4: Model description and simulation of present-day climate, Tech. Rep. 218, Max-Planck-Institut, Hamburg, Germany, 90 pp., 1996. 4992

Schmutz, C., Luterbacher, J., Gyalistras, D., Xoplaki, E., and Wanner, H.: Can we trust proxy-based NAO index reconstructions?, Geophys. Res. Lett., 27, 1135–1138, 2000. 4990

Stephenson, D. B., Wanner, H., Broennimann, S., and Luterbacher, J.: The North Atlantic Oscillation. Climatic significance and environmental impact, Geophys. Monograph Ser., 134, 37–50, 2003. 4989

Taylor, K. E., Stouffer, R. J., and Meehl, G. A.: An overview of CMIP5 and the experiment design, B. Am. Meteorol. Soc., 93, 485–498, 2012. 5003

Trouet, V. and Taylor, A. H.: Multi-century variability in the Pacific North American circulation pattern reconstructed from tree rings, Clim. Dynam., 35, 953–963, 2010. 4990, 5001

Trouet, V., Esper, J., Graham, N. E., Baker, A., Scourse, J. D., and Frank, D. C.: Persistent positive North Atlantic Oscillation mode dominated the Medieval Climate Anomaly, Science, 324, 78–80, 2009. 4990, 5001

Ulbrich, U. and Christoph, M.: A shift of the NAO and increasing storm track activity over Europe due to anthropogenic Greenhouse gas forcing, Clim. Dynam., 15, 551–559, 1999. 4990, 5003

Wallace, J. M. and Gutzler, D. S.: Teleconnections in the geopotential height field during the Northern Hemisphere winter, Mon. Weather Rev., 109, 782–812, 1981. 4989, 4991, 4994, 5012

Wanner, H., Brönnimann, S., Casty, C., Gyalistras, D., Luterbacher, J., Schmutz, C., Stephenson, D. B., and Xoplaki, E.: North Atlantic Oscillation – concepts and studies, Survey Geophy., 22, 321–382, 2001. 4989

Wolff, J. O., Maier-Reimer, E., and Legutke, S.: The Hamburg Ocean primitive equation model HOPE, Tech. Rep. 13, Deutsches Klimarechenzentrum, Hamburg, Germany, 1997. 4992

Woollings, T., Charlton-Perez, A., Ineson, S., Marshall, A. G., and Masato G.: Associations between stratospheric variability and tropospheric blocking, J. Geophys. Res., 115, D06108, doi:10.1029/2009JD012742, 2010a. 5002, 5003

Woollings, T. J., Hannachi, A., Hoskins, B., and Turner, B. A.: A regime view of the North Atlantic Oscillation and its response to anthropogenic forcing, J. Climate, 23, 1291–1307, 2010b. 4989

Yeager, S. G., Shields, C. A., Large, W. G., and Hack, J. J.: The low-resolution CCSM3, J. Climate, 19, 2545–2566, 2006. 4992

Yoshimori, M., Raible, C. C., Stocker, T. F., and Renold, M.: Simulated decadal oscillations of the Atlantic meridional overturning circulation in a cold climate state, Clim. Dynam., 34, 101–121, doi:10.1007/s00382-009-0540-9, 2010. 4993

Zorita, E. and Gonzalez-Rouco, F.: Are temperature-sensitive proxies adequate for North Atlantic Oscillation reconstructions?, Geophys. Res. Lett., 29, 1703, doi:10.1029/2002GL015404, 2002. 4990

Zorita, E., Gonzalez-Rouco, J. F., and Legutke, S.: Statistical temperature reconstruction in a 1000-year-long control climate simulation an excercise with Mann's et al (1998) method, J. Climate, 16, 1378–1390, 2003. 4993

Zorita, E., Gonzalez-Rouco, J. F., von Storch, H., Montavez, J. P., and Valero, F.: Natural and anthropogenic modes of surface temperature variations in the last thousand years, Geophys. Res. Lett., 32, L08707, doi:10.1029/2004GL021563, 2005. 4993

**Table 1.** Overview of simulations available for the analysis.

| Model | Experiment | forcing | Ensemble members | model years |
|---|---|---|---|---|
| CCSM3 | Ctrl1990 | perpetual 1990 AD conditions | 1 | 400 yr |
| CCSM3 | Ctrl1500 | perpetual 1500 AD conditions | 1 | 600 yr |
| CCSM3 | Ctrl1000 | perpetual 1000 AD conditions | 1 | 1200 yr |
| CCSM3 | TR1a-TR4a | transient forcing (see Fig. 1) 1500–2098 AD* | 4 | 598 yr |
| CCSM3 | TR1b | transient forcing (see Fig. 1) 1000–2098 AD* | 1 | 1098 yr |
| ECHO-G | Ctrl1990 | perpetual 1990 AD conditions | 1 | 1000 yr |
| ECHO-G | ErikI/II | transient forcing (see Fig. 1) 1000–2099 AD* | 2 | 1099 yr |

* Note that the transient simulations with CCSM3 and one simulation with ECHO-G use the A2 SRE scenarios for the future (see text for details).





CPD
9, 4987–5018, 2013

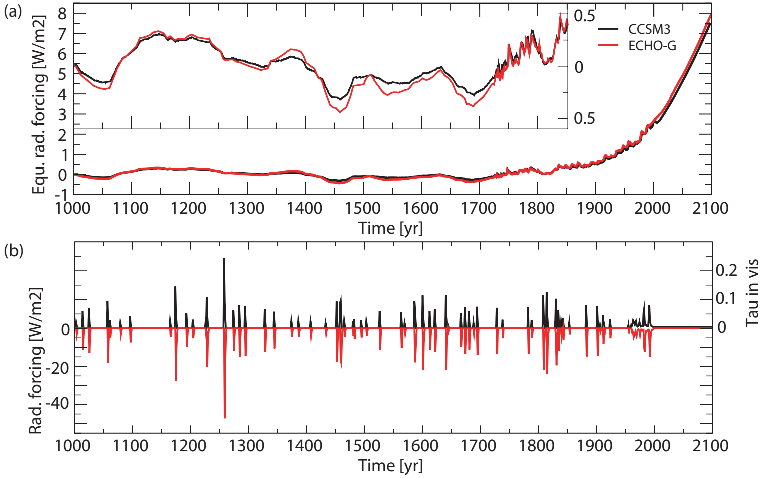


**Fig. 1.** Forcing from 1000 to 2100 AD for the CCSM3 (black) and the ECHO-G (red) transient simulations: **(a)** solar and equivalent $CO_2$ forcing (including $CO_2$, $CH_4$, and $N_2O$) and **(b)** the forcing representing volcanic eruptions. The forcing in (a) is represented after conversion to the equivalent radiative forcing assuming a planetary albedo of 0.31 and using the simplified formula given in IPCC (2001, Table 6.2). The inset in **(a)** focusses on the forcing functions from 1000 to 1850 AD. In **(b)** the optical depth in visible band represents the volcanic forcing of the CCSM3 simulations, whereas in ECHO-G the volcanic forcing is just implemented by changes of the solar constant.





CPD
9, 4987–5018, 2013

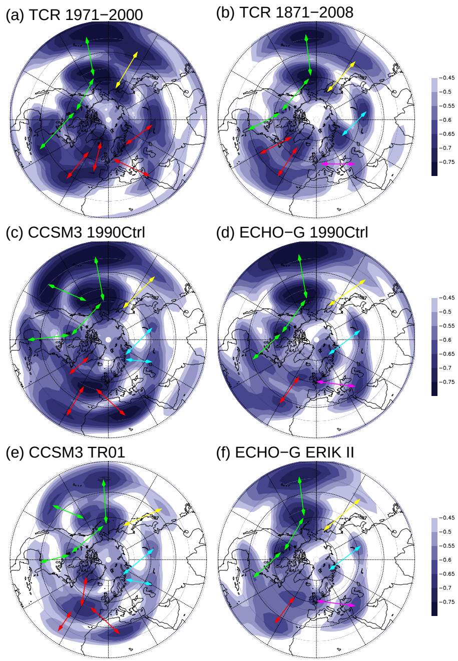


**Fig. 2.** Teleconnectivity based on the 500 hPa geopotential height: **(a)** TCR for the reference period 1971–2000, **(b)** TCR for the period 1871-2008, **(c)** Ctrl1990 of CCSM3, **(d)** Ctrl1990 of ECHO-G, **(e)** TR1a, and **(f)** Erik II. Note that other simulations TR2a – TR4a and TR1b show a similar pattern as **(e)** and Erik I resembles the pattern of **(f)**, therefore they are not shown. The arrows illustrate teleconnection axes and are estimated by one-point correlations in each of the centers of action, as suggested by Wallace and Gutzler (1981) and Raible et al. (2006). They show NAO-type (red), PNA-type (green), and WP-type (yellow) patterns as well as a pattern over Siberia (cyan) and a pattern connecting the eastern Mediterranean with Central Europe (magenta).





CPD
9, 4987–5018, 2013

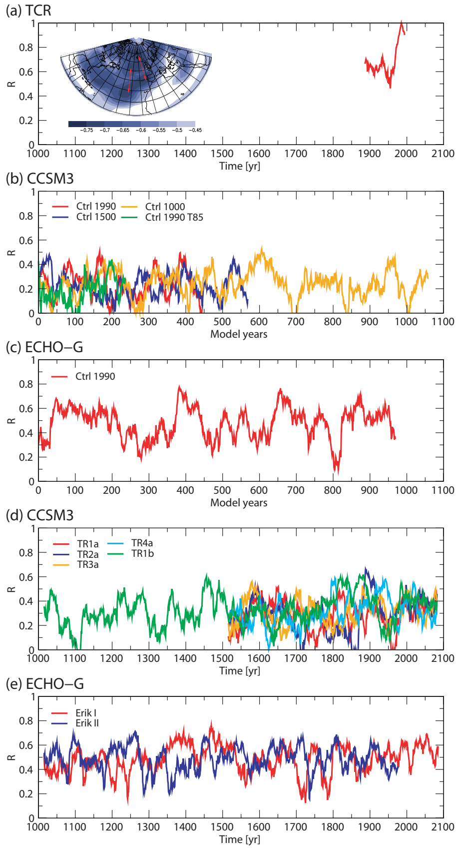


**Fig. 3.** Running spatial correlation time series using a 30 yr window and the reference teleconnectivity pattern (inset in a) for the Atlantic: **(a)** TCR 1871 to 2010, **(b)** CCSM3 Ctrl simulations, **(c)** Ctrl1990 of ECHO-G, **(d)** transient simulations with CCSM3, and **(e)** transient simulations with ECHO-G.





CPD
9, 4987–5018, 2013

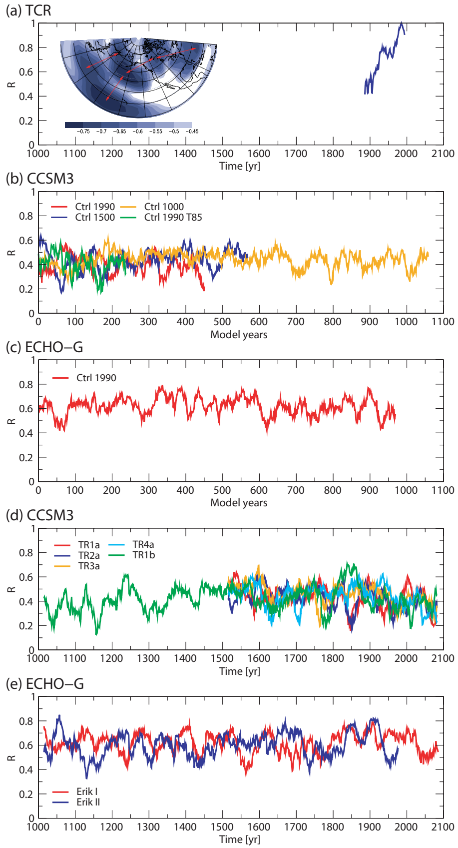


**Fig. 4.** As Fig 3, but for the Pacific (see inset in a).

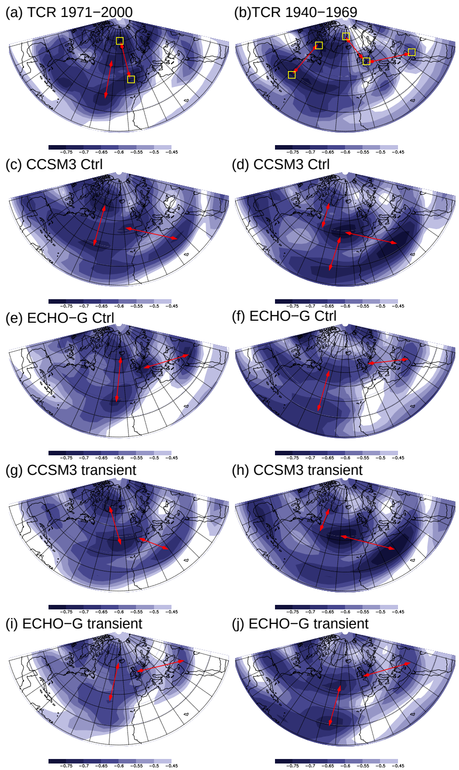


**Fig. 5.** Composites of teleconnectivity for all periods with high (left) and low (right) spatial correlation in the Atlantic: **(a)** TCR period 1971–2000, **(b)** TCR period 1880–1909, **(c, d)** composites of all CCSM3 Ctrl simulations, **(e, f)** composites of the ECHO-G Ctrl1990 simulation, (g,h) composites of all CCSM3 transient simulations and **(e, f)** composites of all ECHO-G transient simulations. Note that the composites are selected according to a distance of at least two standard deviations from the mean of the corresponding spatial correlation times series of Fig. 3. The yellow squares show the location for the index definition in Sect. 4.





CPD
9, 4987–5018, 2013

Changing correlation structures of the NH atmospheric circulation

C. C. Raible et al.

Title Page
Abstract | Introduction
Conclusions | References
Tables | Figures
◄ | ►
◄ | ►
Back | Close
Full Screen / Esc
Printer-friendly Version
Interactive Discussion

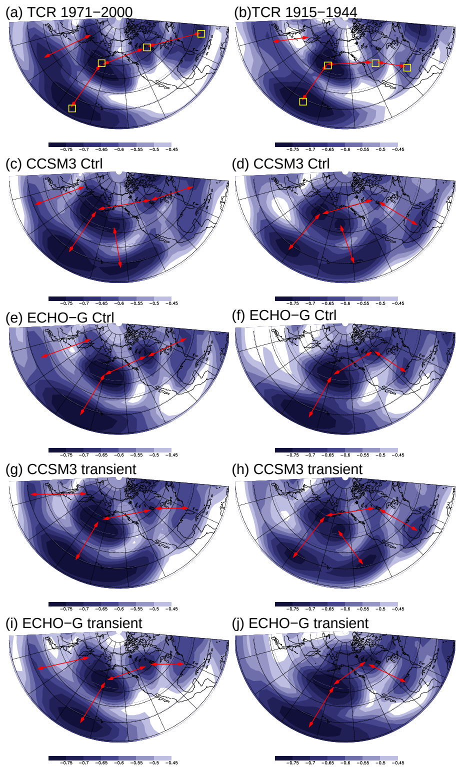


**Fig. 6.** As Fig 5, but for the Pacific.





CPD
9, 4987–5018, 2013

Changing correlation structures of the NH atmospheric circulation

C. C. Raible et al.

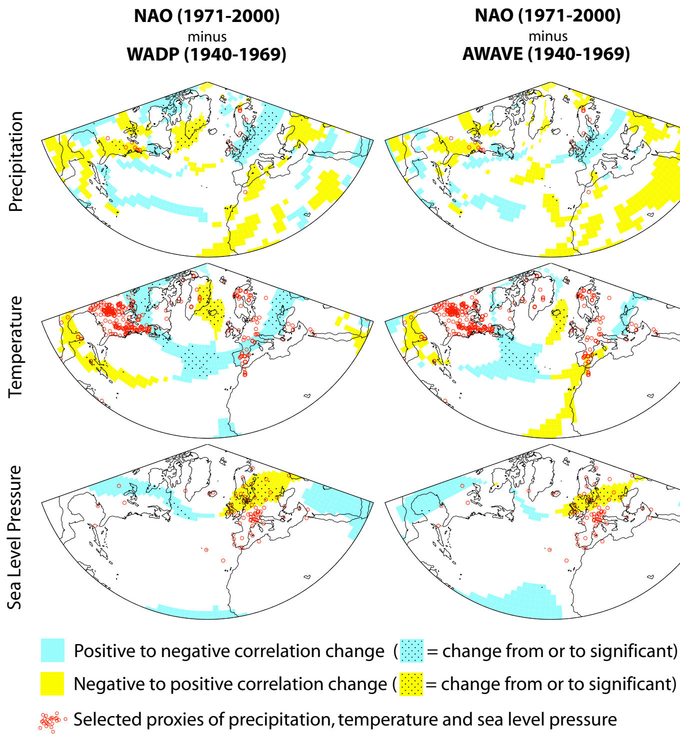


**Fig. 7.** Map indicating where a change in sign occurs in the correlation of an atmospheric circulation index with precipitation, temperature, or sea level pressure if one subtracts the December-February correlation structure of WADP from the one of NAO (left), and of AWAVE from the one of NAO (right). Stippling indicates where a sign change occurs from or to a significant correlation (5 % level in a two-sided *t* test). Selected proxies that have been used in reconstructions of atmospheric circulation are indicated by red circles (see text for details).

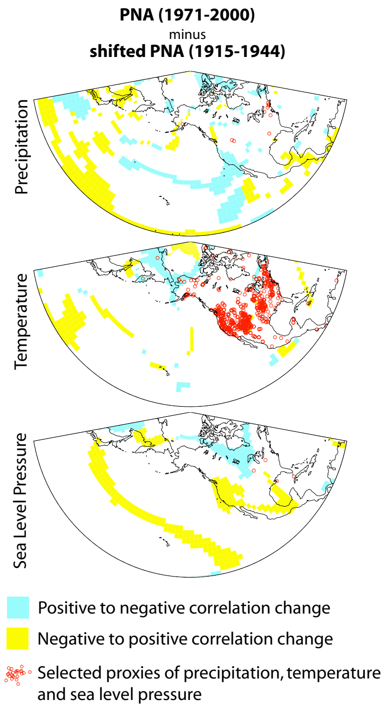


**Fig. 8.** Map indicating where a change in sign occurs in the correlation of an atmospheric circulation index with precipitation, temperature, or sea level pressure if one subtracts the December-February correlation structure of the shifted PNA from the one of the classical PNA. Stippling indicates where a sign change occurs from or to a significant correlation (5 % level in a two-sided *t* test). Selected proxies that have been used in reconstructions of atmospheric circulation are indicated by red circles (see text for details).